

Lawrence Berkeley National Laboratory

Advanced Light Source

Title

Effect of Interconnect Plasticity on Soldering Induced Residual Stress in Thin Crystalline Silicon Solar Cells

Permalink

<https://escholarship.org/uc/item/7r20v58k>

ISBN

9781509043682

Authors

Tippabhotla, Sasi Kumar
Radchenko, Ihor
Song, Wenjian
et al.

Publication Date

2016-11-01

DOI

10.1109/eptc.2016.7861579

Peer reviewed

Effect of Interconnect Plasticity on Soldering Induced Residual Stress in Thin Crystalline Silicon Solar Cells

Sasi Kumar Tippabhotla¹, Ihor Radchenko¹, Wenjian Song¹, N. Tamura², Andrew A. O. Tay¹, A. S. Budiman^{1,*}

¹Singapore University of Technology and Design, Singapore 487372

²Advanced Light Source (ALS)
Lawrence Berkeley National Laboratory (LBNL), Berkeley, CA 94720.

*suriadi@alumni.stanford.edu

Abstract

Soldering of copper interconnects at ~220 °C induces residual stresses in the crystalline silicon (c-Si) solar cells. These residual stresses may become detrimental in the context of thinner silicon cells (< 180µm) causing cracking, performance loss and failures. In such a scenario a systematic evaluation of these residual stresses considering realistic material properties is required to evaluate the risk levels. In the present work, soldering induced residual stresses in the back contact c-Si solar cells were evaluated using finite element simulations. Effect of plasticity of the copper interconnects on the cell residual stress was studied. It was observed that the linear elastic material property of the interconnect over predict the cell stress significantly and hence elastic-plastic material properties are needed for realistic predictions. Simulated stresses were also compared with those of Synchrotron X-ray Micro-diffraction experiments for cell thickness of 180µm to validate the finite element model. Further residual stress was evaluated as a function of silicon cell thickness in order to evaluate the limiting thickness at which the current soldering process and design is no longer failsafe. These results are expected to enable optimization of soldering and interconnect parameters to mitigate high residual stress and thereby cell fractures.

1. Introduction

Despite being the most dominating in the field, the crystalline silicon (c-Si) photovoltaic (PV) technology has widely reported reliability issues due to brittle nature of crystalline silicon. International Energy Agency (IEA) review on failures of photovoltaic modules

revealed that ~10% of the failures are due to cell interconnects [1]. In the PV modules, individual c-Si cells are interconnected using copper ribbons by soldering. Soldering process requires high temperatures close to 220 °C, which induces residual stresses in the components due to CTE mismatch [2-5]. These residual stresses may lead to micro cracks in the c-Si cells or cause fracture of the cells due to propagation of existing cracks [2-5]. Recent technological improvements to reduce cost are driving thinner silicon wafers, which in turn intensify these thermo-mechanical residual stresses [2-4]. Hence a systematic evaluation of the soldering induced residual stresses is necessary to assess the risk levels and device mitigation plans. Finite element analysis (FEA) is being widely used to simulate mechanical failures of c-Si solar PV modules at a lower cost (compared to experiments) with reasonable accuracy and ease [6-12]. However realistic material properties need to be used in FEA simulations to get meaningful results. In the present work soldering induced residual stress in a back contact (for ex. Sunpower) mono crystalline silicon solar cell was simulated using FEA. Effect of elastic vs. elastic-plastic properties of the copper interconnect and solder material on the residual stress was studied. Further the effect of cell thickness reduction on the residual stress was also evaluated using parametric FEA simulations. The simulation results were also validated against the experimental results obtained from Synchrotron X-ray Micro-diffraction (μ SXRD) [13-19] for a nominal cell thickness (180 μ m).

2. Finite Element Modeling and Analysis

Figure 1 shows schematic of the soldered back contact mono crystalline silicon solar cell, analyzed in this manuscript. Each cell was soldered at 3 locations to a typical dog-bone interconnect made of tin coated copper ribbon and the nominal dimensions of the components were also shown in Figure 1. An FEA model shown in Figure 2 was developed based on these dimensions using commercial FEA code, ABAQUS [20]. The FEA model assumes symmetry about the central axis along the length of the copper interconnect and hence only 1 cell and half of the interconnect was modeled as shown. In order to make the model computationally inexpensive, intricate geometric details (ref. Figure 3) of the copper interconnect were omitted and solder joint was idealized to be under the interconnect tab as shown in Figure 2. Back metallization of the cell (ref. Figure 3) was not considered due associated modeling difficulties and unavailability of the geometric parameters. Its effect was assumed to be the same in all the cases studied in this manuscript. The model was meshed with 8 node linear quadrilateral elements with element area of ~0.3 mm² around the solder joint and the cell thickness (180 μ m) was divided into 6 layers as shown to capture local high stresses in the c-Si cell. Anisotropy of the silicon elasticity was considered as given by Eqn (1) [21] and the elastic material properties of the cell, interconnect and solder was given in Table 1 [9-10, 22].

$$\text{Elasticity tensor of c-Si } \langle 100 \rangle, C = \begin{bmatrix} 166 & 64 & 64 & 0 & 0 & 0 \\ 64 & 166 & 64 & 0 & 0 & 0 \\ 64 & 64 & 166 & 0 & 0 & 0 \\ 0 & 0 & 0 & 80 & 0 & 0 \\ 0 & 0 & 0 & 0 & 80 & 0 \\ 0 & 0 & 0 & 0 & 0 & 80 \end{bmatrix} \quad (1)$$

As explained in the previous section, elastic-plastic behavior of the interconnect and solder was also considered in this analysis and the respective plastic properties were given in Table 2 [10, 23]. The model was constrained at the bottom most node of the cell below the middle solder joint to arrest rigid body motion. The CTE mismatch was simulated by steady state response of the model from uniform soldering temperature of 210 °C to room temperature, 25 °C.

3. Experimental

Solar cell sample of nominal thickness $\sim 180 \mu\text{m}$ as shown in Figure 3 was subjected to μSXR D. Detailed experimental procedure was discussed elsewhere [13-14] and Further details on μSXR D technique, Synchrotron X-ray beam and data analysis can be had from references [15-19]. From the data analysis of μSXR D scan [18], the mis-orientation angles (φ_x, φ_y) of the c-Si wafer with respect to the undeformed wafer mid plane (XY plane) were obtained. Then curvatures of the wafer (κ_{xx}, κ_{yy}) with respect to X and Y-axes can be calculated as shown in Equations (2) and (3).

$$\kappa_{xx} = \left. \frac{-\partial \varphi_y}{\partial x} \right|_{y=\text{const}}, \varphi_y \text{ in radians} \quad (2)$$

$$\kappa_{yy} = \left. \frac{\partial \varphi_x}{\partial y} \right|_{x=\text{const}}, \varphi_x \text{ in radians} \quad (3)$$

Using assumptions similar to Kirchhoff plate model [23], the bending strains of the silicon cell can be calculated from curvatures as shown in Equations (4) and (5).

$$\varepsilon_{xx} = \frac{-t}{2} \kappa_{xx}, \text{ where 't' is thickness of the silicon cell and} \quad (4)$$

$$\varepsilon_{yy} = \frac{-t}{2} \kappa_{yy} \quad (5)$$

Since the silicon cell is very thin, assuming the through thickness normal stress (σ_{zz}) to be zero let us calculate the cell bending stresses (σ_{xx}, σ_{yy}) using Hooke's law. The results were presented in the following sections.

4. Results and Discussion

Stress contours in the 180 μm thick c-Si cell surrounding the solder joint considering both elastic and elastic-plastic material properties were shown in Figure 4. It can be noticed that the stresses are concentrating around the solder joint and high in-plane stresses are seen with elastic material properties which reduced significantly upon using elastic-plastic material properties for copper interconnect and solder. The maximum X-direction stress with elastic properties was 176 MPa, which reduced to 133 MPa upon incorporating copper interconnect plasticity and further reduced to 81 MPa upon incorporating solder material plasticity. The reduction of stress is very significant (>50%) and can't be ignored. Similarly the Y-direction stress reduced from 99 MPa to 69 MPa (>30% reduction). Figure 5 shows the experimental stress maps obtained by μSXR D of 180 μm thick back contact mono crystalline silicon cell. The FEA stress contours with elastic plastic material properties (Figure 4c) compare well with the experimental stress maps and this validates our FEA model. These results also show that the plasticity (or ductility) of the interconnect and solder play crucial role in reducing soldering induced stresses. An alloy material, which is less stiff and more ductile, compared to copper may be a better choice for interconnection to reduce stresses. Or it may be even better to engineer such material. Further in this manuscript the effect of silicon cell and interconnect thickness on the cell residual stress was simulated (Figure 6). It can be seen from Figure 6a that the X-direction stress is increasing almost linearly with reduction in cell thickness and the Y-direction stress is reducing, which in turn increases the in plane max principal stress, hence tendency to fracture. However decreasing the copper interconnects thickness can counterbalance the reduction in cell thickness. It can be seen from Figure 6b that the stresses reduce due to reduction interconnect thickness. Similarly the thickness of the solder may also affect the residual stresses, which was not studied in this manuscript.

5. Conclusions

The effects of copper interconnect and solder plasticity on the silicon cell residual stress simulated using FEA. The residual stress depends significantly on the interconnect plasticity and hence a less stiff and ductile alloy may become a better choice for solar cell interconnection. The FEA results match well with the experimental results. Further the effect of silicon wafer (cell) thickness on the cell residual stress was also evaluated to show that residual stress in the cell increases linearly with cell thickness. Further it was noticed from the simulations that the reduction in cell thickness can be counterbalanced by the reducing the interconnect thickness to curtail stress levels. These preliminary results are encouraging and inspire us to evaluate the residual stresses holistically including lamination process with interconnect and solder material plasticity, reduced cell thickness etc. to optimize the interconnection process and topology for a more reliable solar PV technology.

Acknowledgements

The authors gratefully acknowledge the samples and support provided by Dr. Alexander Caldwell of SunPower for the Synchrotron X-ray Microdiffraction experiments.

Authors also also gratefully acknowledge the funding and support from National Research Foundation (NRF)/Economic Development Board (EDB) of Singapore for the project under EIRP Grant “(NRF2013EWT- EIRP002-017) - Enabling Thin Silicon Technologies for Next Generation, Lower Cost Solar PV Systems”

The Advanced Light Source (ALS) (supported by the Director, Office of Science, Office of Basic Energy Sciences, and Materials Sciences Division, of the U.S. Department of Energy under Contract No. DEAC02-05CH11231 at Lawrence Berkeley National Laboratory and University of California, Berkeley, California). The move of the micro-diffraction program from ALS beamline 7.3.3 onto to the ALS superbend source 12.3.2 was enabled through the NSF grant #0416243.

References

1. “Review of Failures of PV Modules”, Report: IEA-PVPS T13-01:2014, Photovoltaic Power Systems Program, International Energy Agency. (<http://www.iea-pvps.org/index.php?id=275>).
2. A. Gabor, M. Ralli, S. Montminy, L. Alegria, C. Bordonaro, J. Woods, L. Felton, Soldering induced damage to thin Si solar cells and detection of cracked cells in modules, in: Proceedings of EUPVSEC, 2006.
3. I.J. Bennet et al., “Low-Stress Interconnection of Solar Cells”, 22nd European Photovoltaic Solar Energy Conference and Exhibition, Milan, Italy, 3-7 september 2007.
4. Pingel S, Zemen Y, Geipel T, Berghold J. Mechanical stability of solar cells within solar panels. Proc. 24th European Photovoltaic Solar Energy Conf., Hamburg, Germany; 2009, pp. 3459-3463.
5. J. Wendt, M. Träger, M. Mette, A. Pfennig, B. Jaeckel, The link between mechanical stress induced by soldering and micro damages in silicon solar cells, in: Proceedings of EUPVSEC, 2009, pp. 3420–3423.
6. S. Dietrich, M. Pander, M. Sander, S.H. Schulze, and M. Ebert. Mechanical and Thermo-Mechanical Assessment of Encapsulated Solar Cells by Finite-Element-Simulation. Proceedings of SPIE –The International Society for Optical Engineering, 2008.
7. M. Sander, S. Dietrich, M. Pander, S. Schweizer, M. Ebert, and J. Bagdahn, “Investigations on crack development and crack growth in embedded solar cells”, Proceedings of SPIE –The International Society for Optical Engineering, 2011.
8. S. Dietrich, M. Pander, M. Sander, and M. Ebert. “Mechanical investigations on metallization layouts of solar cells with respect to module reliability”, Energy Procedia 38 (2013) 488 – 497.
9. Ulrich Eitner, Thermomechanical Analysis of Photovoltaic Modules, PhD

- Thesis, Centre for Engineering Sciences, Martin Luther University of Halle-Wittenberg, Germany, 2011.
10. Osama Hassan et al., "Finite Element Modeling, Analysis, and Life Prediction of Photovoltaic Modules" J. of Solar Energy Engg., Transactions of the ASME, Vol.136,MAY2014.
 11. Y. Lee and A.A. O. Tay. Finite thermal analysis of a solar photovoltaic module. 37th PVSC conf., Seattle, 19-24 June 2011.
 12. Y. Lee and A.A. O. Tay, Stress Analysis of Silicon Wafer Based Photovoltaic Modules in Operation", PV Specialist Conference, Austin, 3-8 June 2012.
 13. A.S. Budiman et al., "Enabling thin silicon technologies for next generation c-Si solar PV renewable energy systems using synchrotron X-ray microdiffraction as stress and crack mechanism probe" Solar Energy Materials & Solar Cells, 2014, Vol. 130, pp. 303-308
 14. Sasi Kumar Tippabhotla et al. , "Synchrotron X-ray Micro- diffraction – Probing Stress State in Encapsulated Thin Silicon Solar Cells", Procedia Engineering, Volume 139, 2016, Pages 123-133.
 15. A.S. Budiman, Probing Crystal Plasticity at the Nanoscales, Springer, 2015.
 16. Kunz, M., Tamura, N., Chen, K., MacDowell, A. A., Celestre, R. S., Church, M. M., ... & Morrison, G. Y. (2009). A dedicated superbend X-ray microdiffraction beamline for materials, geo, and environmental sciences at the advanced light source. Review of Scientific Instruments, 80(3), 035108.
 17. N. Tamura, M. Kunz, K. Chen, R. S. Celestre, A. A. MacDowell, and T. Warwick. A superbend X-ray microdiffraction beamline at the advanced light source. Materials Science and Engineering A-structural Materials Properties Microstructure and Processing, 524:28–32, 2009.
 18. N. Tamura, H. A. Padmore, and J. R. Patel. High spatial resolution stress measurements using synchrotron based scanning X-ray micro- diffraction with white or monochromatic beam. Materials Science and Engineering A-structural Materials Properties Microstructure and Processing, 399:92–98, 2005.
 19. Tamura N., XMAS: A Versatile Tool for Analyzing Synchrotron X-ray Microdiffraction Data, Chapter-4 of Strain and Dislocation Gradients from Diffraction, World Scientific, 2014.
 20. ABAQUS Documentation, Version 6.14, SIMULIA, Dassault Systèmes Simulia Corp., 2015.
 21. V. Kaajakari, http://www.kaajakari.net/~ville/research/tutorials/elasticity_tutorial.pdf (Last accessed, May 2016).
 22. Zhanli Guo et al., Modeling Material Properties of Lead-Free Solder Alloys, J. of Electronic Mat., Vol. 37, No. 1, 2008
 23. B. Yeung et al., Correlation between mechanical tensile properties and microstructure of eutectic Sn-3.5Ag solder, J. Mat. Sc. Letters 21, 2002, 723– 726

Tables

Table 1: Elastic Material Properties [9-10, 22]

Material	Young's Modulus, E		Poisson's Ratio	CTE (mm/mm/deg C)	
	Value	Temperature (deg C)		Value (PPM)	Temperature (deg C)
Silicon	Eqn (1)	---	0.28	1.72	-53
				2.23	-13
				2.61	27
				3.34	147
Copper (Interconnect)	91.5	-40	0.3	17	---
	85.7	25			
	82	125			
	79.2	225			
Solder (Sn-Ag-Cu)	53	0	0.35	21	---
	45	100			
	36	200			

Table 1: Plastic Material Properties [10, 23]

Material	Yield Stress (MPa)	Tangent Modulus (MPa)	Temperature (deg C)
Copper (Interconnect)	116.2	1000	-40
	95.1	1000	25
	82	1000	125
	79.2	1000	225
Solder (Sn-Ag-Cu)	45	-	25
	28	-	180
	25	-	210

Figures

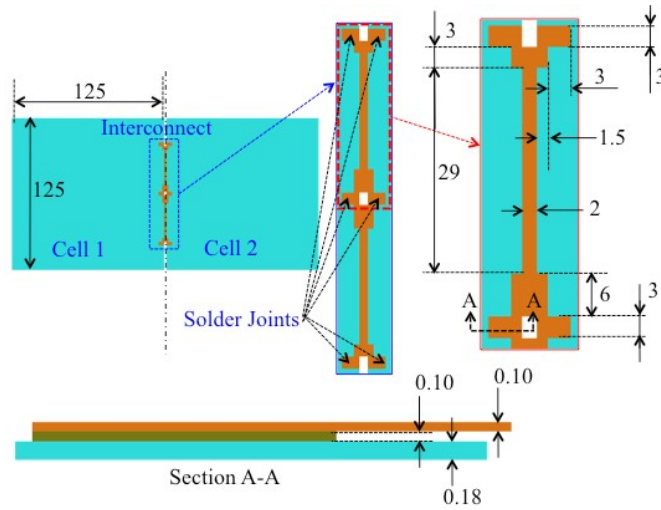


Figure 1: Schematic of Soldered Silicon Cells and Dimensions (not to scale)

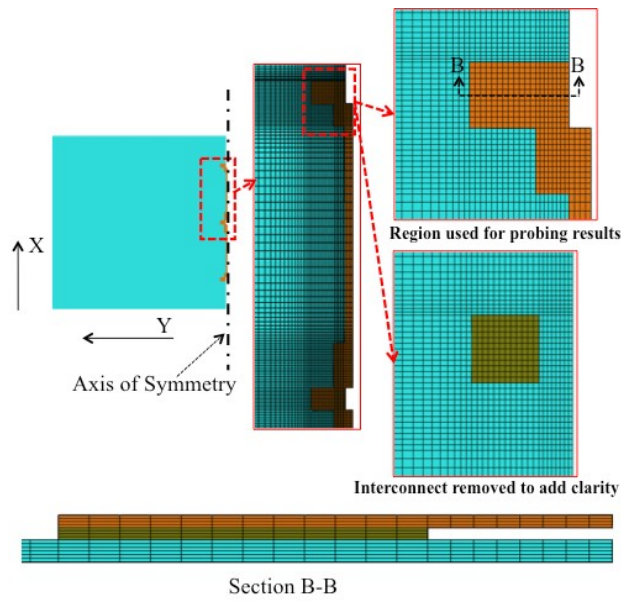


Figure 2: Finite Element Model Details

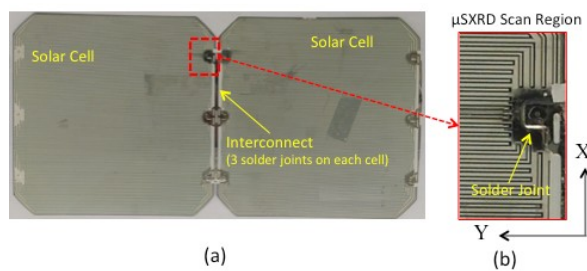


Figure 3: (a) Experimental Sample of the soldered cells, (b) μ XRD scan region

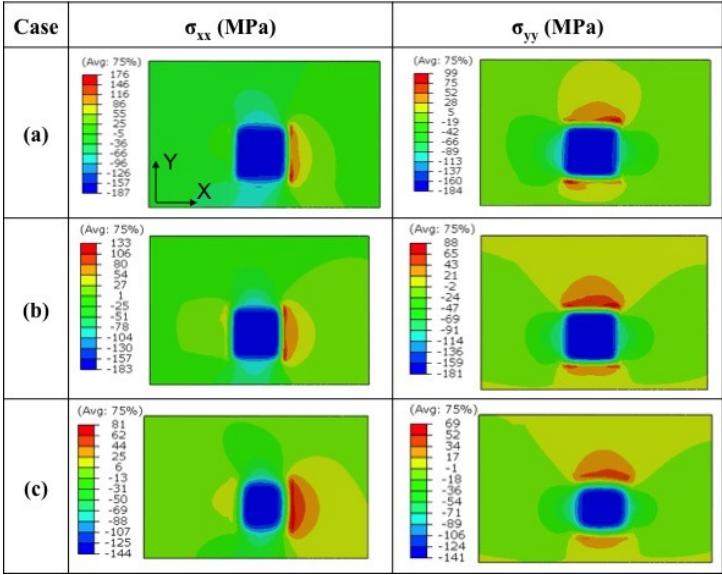


Figure 4: Post soldering residual stresses of 180 μ m thick silicon cell from FEA simulations, (a) with Elastic material properties, (b) with elastic-plastic copper interconnect and elastic solder, (c) with elastic-plastic copper interconnect and solder

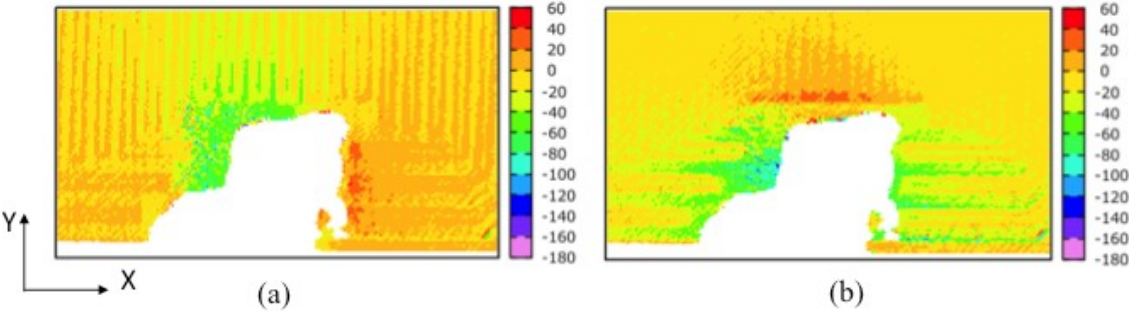
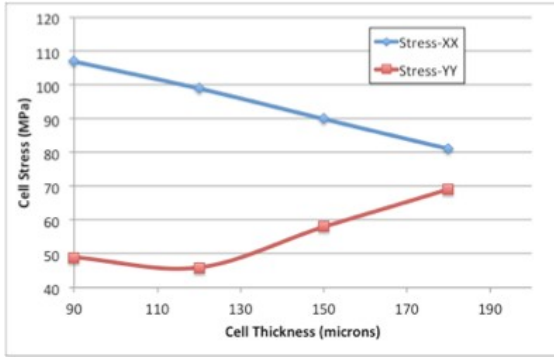
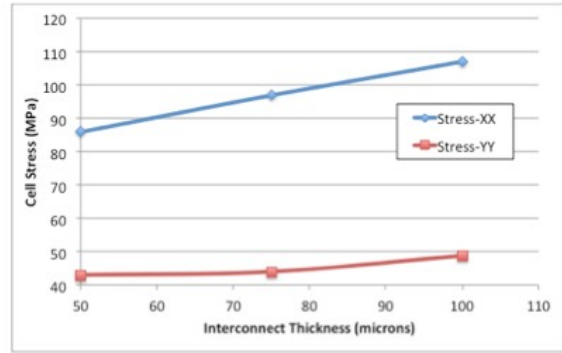


Figure 5: Post soldering residual stresses of 180 μ m thick silicon cell from μ SXRD, (a) X-direction stress, (b) Y-direction stress



(a)



(b)

Figure 6: Post soldering residual stresses of silicon cell from FEA simulations considering elastic-plastic material properties for interconnect and solder, (a) for varying cell thickness, (b) for varying interconnect thickness (cell thickness 90 μm)